ČERVENKA CONSULTING
Červenka Consulting s.r.o.
Na Hrebenkach 55
150 00 Prague
Czech Republic
Phone: +420 220 610 018
E-mail: cervenka@cervenka.cz
Web: http://www.cervenka.cz

User's Manual
digiBeton module for ATENA

Project result FW06010422-V1

Version 3.0

Written by
Jiří Rymeš

Prague, December 2025

Acknowledgements:

*The software module was developed with partial support of **TAČR TREND Programme***

T A

Č R

*("TREND Funding programme for research, experimental development and innovation", project no. FW06010422: "**digiBeton**", Simulation and design of structures from digital concrete)*

CONTENTS

1 INTRODUCTION

The digiBeton module is a newly developed feature enabling simulations of the 3D concrete printing (3DCP) process and the behaviour elements constructed by the 3DCP technology (see Figure 1). This module is integrated within the ATENA software package [1] and enables advanced finite element analysis (FEA) directly from a G-code file produced by a 3D CAD modeller. The module is distributed as an extension of the ATENA Preprocessor software, and its availability within the ATENA software framework is subject to licensing.

3DCP is an additive manufacturing construction technology in which cement-based material is extruded layer-by-layer to fabricate elements without the use of conventional formwork. The process is affected by the material rheology, extrusion dynamics, and layer deposition, resulting in complex geometries. The process is characterised by a time-dependent material response and anisotropic mechanical behaviour. The digiBeton module offers a tool for numerical simulations of 3DCP, enabling both the analysis of the fresh state stability and structural performance after printing.

A typical workflow begins with importing a geometric model in the form of a G-code file that is used for creating a 3D model of a printed object. The G-code file is used for creating a numerical model directly discretised with finite elements (FE). This is followed by the definition of material properties, including time-dependent relationships for the evolution of material parameters. The printing process is then simulated through layer-by-layer material deposition, accounting for kinematics and boundary conditions. Finally, the resulting as-printed structure can be used as input for structural analysis to evaluate its mechanical response, stability, and performance under prescribed loading scenarios.

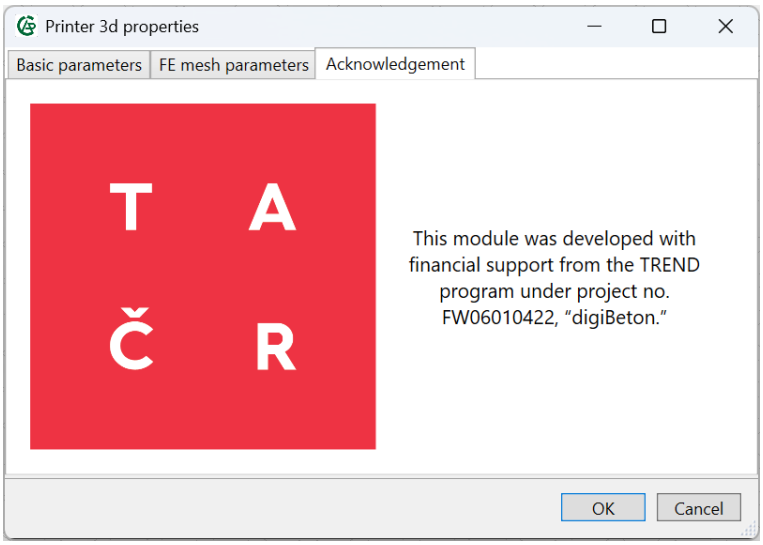

Figure 1: Project acknowledgement after module activation.

2 ANALYSIS OF FUNCTIONAL REQUIREMENTS

The aim of the module is to offer an advanced tool for simulation and quality control in the development and design of construction structures made using the 3DCP technology. Digital fabrication of structures using additive manufacturing, namely 3D printing, has become one of the most dynamic research areas in civil engineering in recent years, driven by the need for more efficient, sustainable, and design-flexible construction technologies. The presented module aims to significantly elevate the current technological level in the numerical analysis of the 3DCP structures.

The main requirement of the module is to represent a simulation-based technological tool that is accessible, robust, and practically usable for a broad spectrum of the engineering community, including researchers, designers, and practitioners. Emphasis is placed on the seamless connection between CAD design and direct structural performance assessment, enabling informed decision-making throughout the design process of a 3D-printed object. A schematic overview of the module's usage is shown in Figure 2.

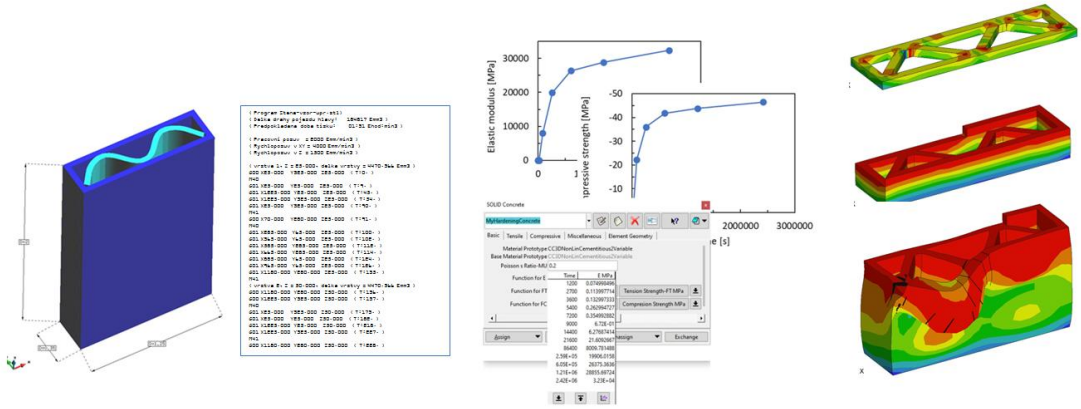

Figure 2: Schematic illustration of the usage of the digiBeton module.

The primary stakeholders of the module include software developers, researchers in digital construction and material science, civil and structural engineers, and technology providers involved in 3DCP hardware and materials. Target users are simulation engineers, designers of 3D-printed concrete structures, and researchers performing numerical and experimental validation of process and material models.

For practical application in engineering practice, targeted research and development are required in the following key areas:

- generation of the FE numerical model based on the G-code output,
- availability of a suitable material model enabling a realistic simulation of the material response during the early age and evolution of material performance characteristics in time,
- methods for verification of the final structure with respect to the original digital design and manufacturing parameters.

The module is assumed to operate as part of a larger software franework, with input data originating from CAD or slicing tools and with extensible material models. Key constraints include the need for computational efficiency suitable for engineering workflows, compatibility with established data formats such as G-code, and a modular architecture that supports long-term maintainability and future development.

The functional requirements of the module are organised into thematic categories reflecting the main aspects of the 3DCP workflow, namely data input and integration, process and toolpath simulation, material modelling and time-dependent behaviour, and structural performance and safety assessments. Furthermore, the simulation framework needs to be able to assess the specifics of the 3DCP technology, such as the interlayer bond, which is not typically dominant for other areas of concrete technology.

The module shall simulate the layer-by-layer extrusion process based on toolpath definitions and process parameters, represent key printing variables such as nozzle geometry, extrusion rate, and printing speed, and identify potential process-related issues, including collisions, instabilities, or unsupported printed segments.

3 TECHNICAL DOCUMENTATION

3.1 Method for accessing stability

A crucial aspect of numerical simulations for the 3DCP process involves capturing the potential loss of stability of the printed element as it is being constructed. This phenomenon arises from the interplay between the evolving material properties and the increasing weight of the structure during the printing process. Freshly deposited material in the lower layers of a 3D-printed element typically exhibits low yield stress, meaning it can deform significantly, even under the self-weight of the structure. As printing progresses and upper layers are added, the weight transferred by these lower layers increases. This combination of low material strength and increasing load may lead to increasing deflection in the structure. In the worst-case scenario, this deflection can progress into buckling collapse, a characteristic failure mode in additive manufacturing techniques like 3DCP.

To accurately assess the risk of stability loss, the ATENA adopts the updated Lagrangian formulation. This method updates the nodal coordinates either after each solution step or iteration based on the calculated deformation. This approach allows the simulation to reflect the time-dependent nature of 3DCP, where the structure continuously deforms under its self-weight as printing progresses. Furthermore, the updated Lagrangian formulation enables the inclusion of second-order effects in the overloading simulation at the mature age. This, also known as P-delta effects, accounts for the influence of the axial load acting on the element with lateral displacement. In the context of 3DCP, this becomes relevant as the deformation occurring during the printing process.

A key aspect of this approach lies in its ability to simulate the actual construction process. Unlike traditional static analyses, where loads are applied instantaneously, nonlinear FEM employs a step-by-step approach. In this method, the loads are incrementally increased over several steps, allowing the development of nonlinear material behaviour, which typically results in the redistribution of the internal forces. For 3DCP, each step in the simulation is assigned to a specific time during the printing process. Then, during the simulation run, a group of elements is activated at each step according to the printing speed and trajectory, simulating the actual construction method. The moment of an element's activation, referred to as the element construction time, is a key variable that is further used at each solution step for the estimation of the loads and material model parameters. This allows simulation of the material maturing and shrinkage. This step-wise approach with time-dependent load application provides a more realistic picture of the stresses and strains developing within the structure as it is being printed.

When nonlinear material laws are introduced into the FEM, the set of equations becomes nonlinear. Therefore, a suitable solver technique is necessary to find the equilibrium between the nodal displacement and material response. This is called convergence of the solution. Most commonly, these methods are derived from the well-known Newton-Raphson method. The iterative solution runs until the residual error is lower than the defined convergence criteria.

Once the convergence at a given load step is obtained, the next load step is calculated based on the previously calculated state. Unlike in the linear (i.e., elastic) solution, the superposition principle is not valid, meaning that the structural response under multiple

loadings cannot be found by simple addition. Therefore, the loading history plays an important role in the simulation and should resemble the actual loading scenario.

3.2 Material models

3.2.1 Concrete material model

Accurately modelling material behaviour is essential for numerical simulations, particularly in 3DCP, where material nature evolves from a thixotropic, non-Newtonian fluid to a solid hardened paste. This example adopts the model of Červenka et al. [2], [3] and extends it with a time-dependent component to simulate the hardening paste used in 3D concrete printing. The material model thus accounts for the gradual increase in material performance. At the moment of printing, the material performance characteristics are primarily determined by the thixotropic nature of the paste. This initial phase can be further divided into two stages. First, the re-flocculation phase occurs when the interparticle bonds are re-created, leading to a slight increase in strength. The second mechanism is the formation of the early hydration products, referred to as the structuration phase. For small-scale samples that are printed in the time frame of a few hours, these two mechanisms are dominant during the printing process, and the hydration after the dormant period hardens the paste already in the final shape.

In the numerical analysis, as the paste hardens, the parameters in the material model are updated for each finite element at each solution step to reflect the evolving state of the material. Each integration point within the model has unique material parameters that are updated at each solution step to reflect the ongoing hardening process based on the element construction time.

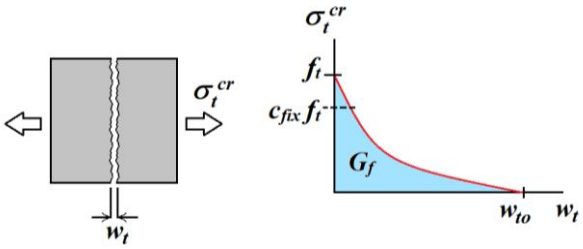

Figure 3: The fracture energy softening law controlling the crack opening in tension.

The fracture-plastic model proposed by Červenka J. et al. [2], [3] divides the nonlinear material response into tension and compression. The tensile post-peak response is characterised by an orthotropic smeared crack model with a softening curve controlled by the fracture energy that is dissipated during the crack formation, as shown Figure 3. The fracture process is simulated using the so-called smeared crack approach. Rather than explicitly tracking each individual crack, the smeared crack approach adds the response of multiple cracks within a single element and adequately reduces the strength of the element. The cracking model is orthotropic and allows the formation of up to three cracks in the three principal directions.

The compression branch is described by the plasticity approach with the Menetrey & Willam failure criterion [4] as shown in Figure 4. After exceeding the stress level corresponding to the onset of crushing, hardening is simulated, followed by linear softening after exceeding the compressive strength. The material model incorporates a yield surface and flow rule to capture the compressive plasticity of the material.

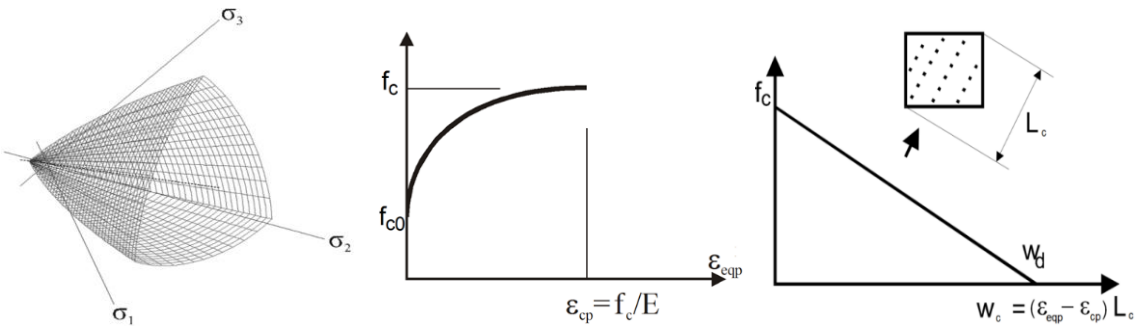

Figure 4: The Menetrey & Willam failure criterion used in compression, and the hardening and softening laws for concrete crushing.

3.2.2 Interface material model

The connection between the adjacent layers of concrete can be simulated using an interface material model utilising the Mohr–Coulomb model. It is a failure criterion used for describing frictional and cohesive behaviour at material discontinuities. The Mohr–Coulomb criterion limits the admissible shear traction as a function of the normal stress and friction coefficient, allowing frictional sliding with or without cohesion. The Mohr-Coulomb material model is schematically illustrated in Figure 5.

In the tensile branch, a tension cut-off is introduced by prescribing a maximum allowable normal stress, physically representing the tensile strength of the interface. Once this tensile limit is exceeded, the interface loses its load-carrying capacity in the normal direction, representing debonding.

To capture progressive degradation, the model uses a softening law, in which the cohesion and tensile strength decrease with increasing slip or opening, respectively. This enables simulation of gradual interfacial damage, reduced load transfer, and eventual separation, which are essential for modelling interlayer bonding and failure mechanisms. Capturing this mechanism is essential for modelling failure zones between the deposited layers of concrete.

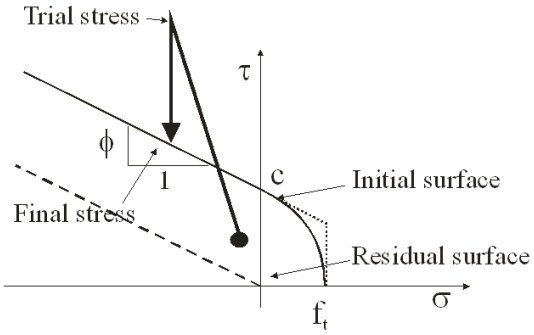

Figure 5: The Mohr-Coulomb material model used for modelling interfaces between concrete layers.

4 PROGRAMMING DOCUMENTATION

This section describes the implementation 3DCP module into the overall ATENA software framework. It is illustrated in Figure 6.

First, a G-code file for an object is chosen through a dedicated module's dialogue in the ATENA Preprocessor environment. ATENA Preprocessor represents the main graphical user interface (GUI) for controlling the module. Together with several model parameters, the target G-code file is sent to the ATENA Core, where a full 3D FE model is created by the CCGenerate library. The model data are sent back to the ATENA Preprocessor for visualisation. This implementation strategy allows users to review and eventually refine the FE model right at the beginning of the model development.

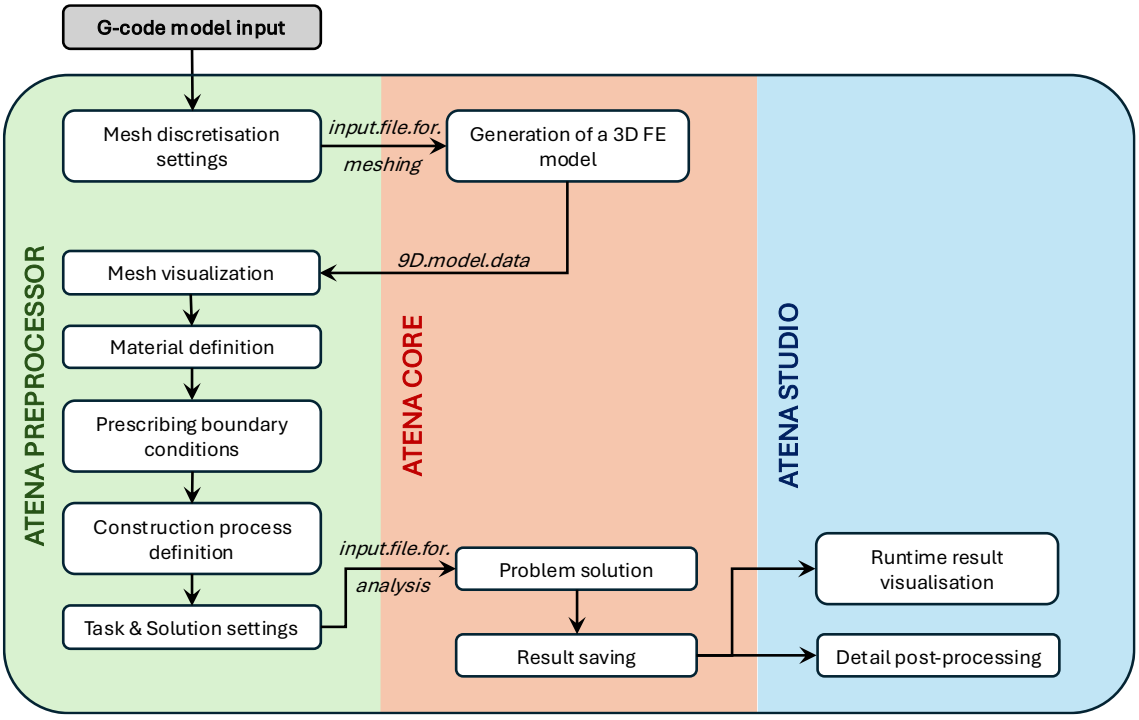

Figure 6: Schematic of the module implementation within the ATENA software framework.

After the model generation, the workflow in the module is analogous to the general modelling procedure in ATENA Preprocessor, thus, the existing software's infrastructure is used. This includes mainly material definition and boundary conditions dialogues and menus. These, however, contain newly developed material libraries and prototypes in the form of XML templates and Python scripts as illustrated in Figure 7.

A feature specifically dedicated to 3DCP simulation is an input dialogue for additive manufacturing, controlling the construction process. It contains a definition of the printing path – a trajectory over which the finite elements of the model are gradually activated to simulate the actual construction method. This can be either inherited from the initial G-code input or can be redefined to assess the model's behaviour under different printing scenarios. The printing path can also be input as a direct set of coordinates in the form of a CSV file.

The entire GUI pre-processing input can be replaced by a script. An example of a script is given in the appendix of this document.

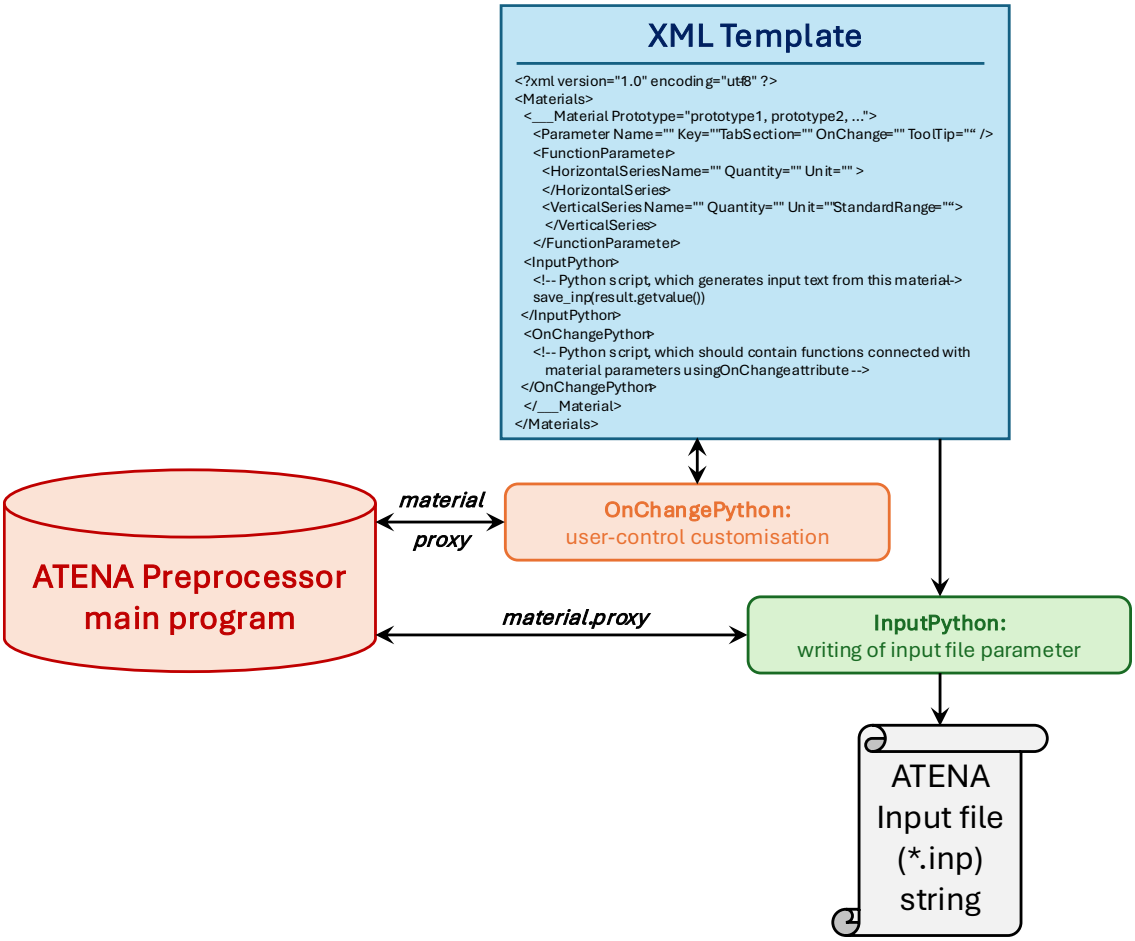

Figure 7: Schematic diagram of XML templates with Python scripts implemented for material inputs.

The final step of pre-processing is the generation of an analysis input file, after which the solution is launched. The input file contains a set of instructions for the ATENA Core that are evaluated to solve the problem. As the solution progresses, the results of the calculated steps are gradually stored on the computer's hard drive and can be instantly reviewed even before completion of the entire analysis run. The analysis results are reviewed in ATENA Studio, which serves as a post-processor in the ATENA software framework. ATENA Studio visualises how the model deforms during the printing. Furthermore, a more detailed post-processing can be done by plotting

5 USER MANUAL

5.1 Creating a model

The workflow within the digiBeton module begins with the automatic generation of the FE mesh based on the user-inputted G-code file. In this step, the set of points along the 1D printing trajectory is used for creating a 3D network of finite elements, discretising the simulated object. The model creation dialogue shown in Figure 8 is launched from:

File → Import → Create model from G-code

In this dialogue, the general properties of the model are specified. Mainly, it is the source G-code file and the geometrical proportions, such as the width and thickness of the printed layers. The dialogue also enables activation of the "Variable layer thickness" option, that designed for nonplanar geometries. If activated, the software automatically adjusts the layer's dimensions along the height of the model.

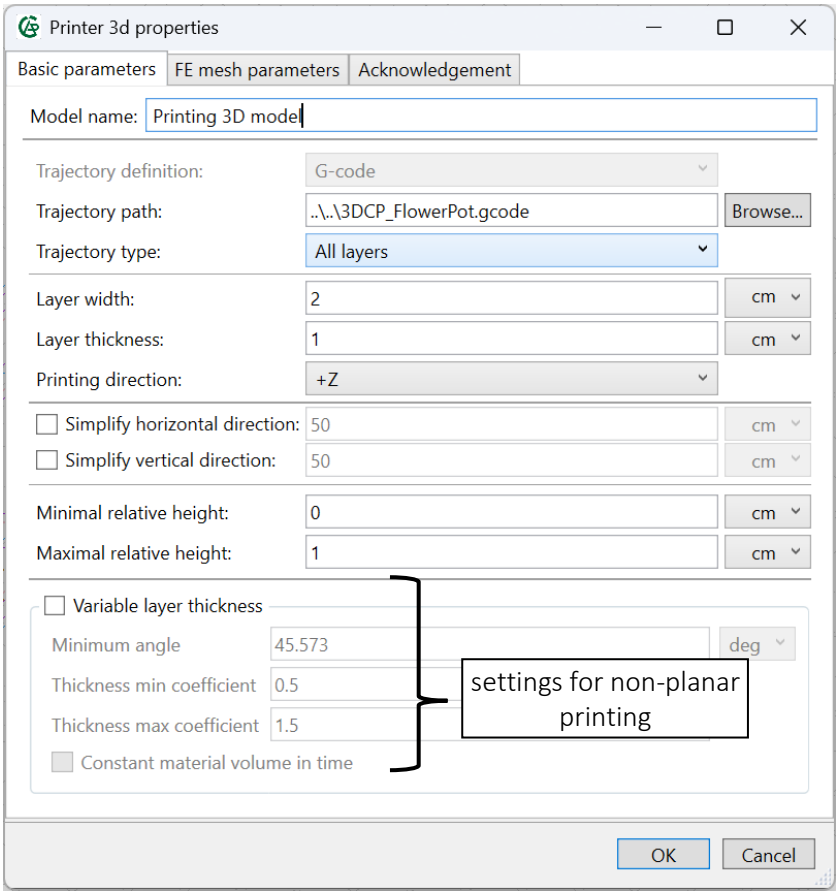

Figure 8: Dialogue window for creating a finite element model from a G-code file.

In the context of 3DCP, a G-code file defines the machine-level instructions required to execute the printing process. It specifies the printing head geometry, layer sequence in terms of spatial coordinates and extrusion control. An example of a compatible G-code file is shown in Figure 9. The G-code file should contain absolute coordinates of the points along the printing trajectory.

```
G00 X82.500 Y0.000 Z5.000
M40 (extruder on)
G01 X135.000 Y0.000 Z5.000
G01 X145.607 Y4.393 Z5.000
G01 X150.000 Y15.000 Z5.000
G01 X150.000 Y135.000 Z5.000
G01 X145.607 Y145.607 Z5.000
G01 X135.000 Y150.000 Z5.000
G01 X15.000 Y150.000 Z5.000
G01 X4.393 Y145.607 Z5.000
G01 X0.000 Y135.000 Z5.000
G01 X0.000 Y15.000 Z5.000
G01 X4.393 Y4.393 Z5.000
G01 X15.000 Y0.000 Z5.000
G00 X82.500 Y0.000 Z5.000
M41 (extruder off)
G00 X82.500 Y-1.000 Z10.000
M40 (extruder on)
G01 X135.000 Y-1.000 Z10.000
G01 X146.314 Y3.686 Z10.000
```

Figure 9: Example of an input G-code input.

The mesh density can be controlled along the printing path (labelled as R-direction), across the layer width (labelled as S-direction) and along the height of the model (labelled as T-direction). The mesh setting dialogue is shown Figure 10. It should be noted that the final mesh FE model is not discretised based on the coordinates, as it may result in very dense meshes not suitable for numerical analyses. On the other hand, in the case of coarse point spacing (e.g., on straight sections), the resulting mesh is refined.

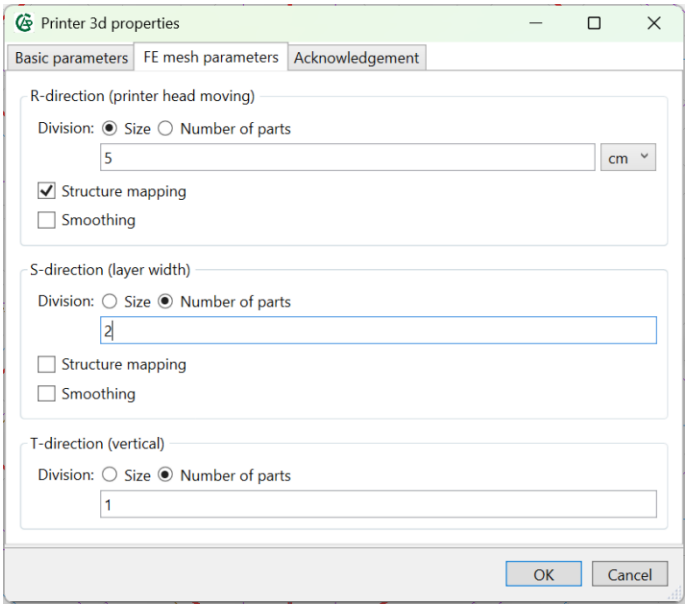

Figure 10: Meshing parameters input for creating a model based on a G-code file.

Upon confirming the dialogue window, the G-code file is processed and the 3D FE mesh is generated using the ATENA core. The final mesh can be immediately reviewed in the ATENA Preprocesor window. Furthermore, a new solid object is created together with the FE model as shown in Figure 11. This solid is represented by a bounded box

surrounding the FE model and is used for prescribing the material properties and boundary conditions.

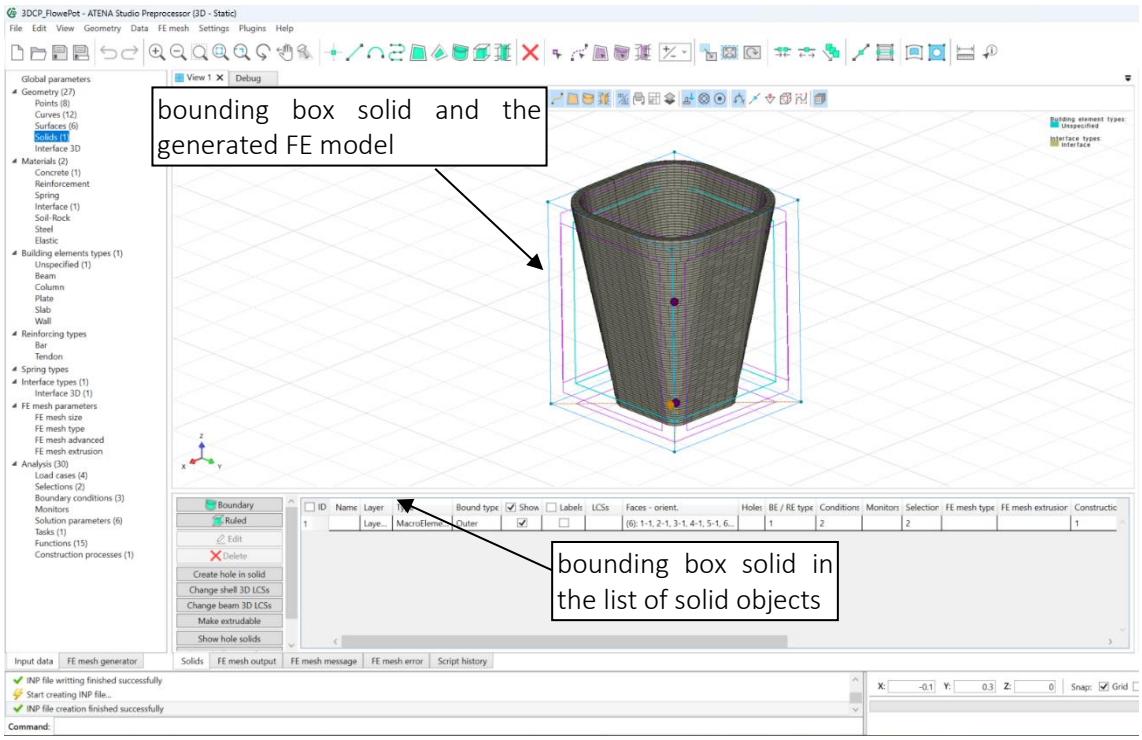

Figure 11: Example of the FE model created from a G-code file. The solid surrounding the FE mesh represents a bounding box used for working with the model.

By repeating the model-creating dialogue, multiple FE models can be created. This is useful for simulations of objects that are composed of multiple segments, each having its own G-code file. Previously created models can be edited through the edit option of the respective bounding box solid object. This is useful, for instance, for mesh refinement.

5.2 Material models

5.2.1 Modelling concrete hardening

As mentioned earlier, the created FE model is in the form of an FE mesh that cannot be directly controlled or accessed through the GUI. Therefore, the material model is prescribed to the bounding box solid.

A suitable material model for 3DCP simulation can be selected from the standard material library in ATENA Preprocessor in the **Materials: Concrete** item in the navigation tree window. The material prototype supporting the variation of material properties during analysis is called **Cementitious2_Variable**. This material prototype allows for variation of the material properties during the analysis run and is available upon changing the default prototype (note that the **Change prototype** checkbox needs to be activated), as shown in Figure 12.

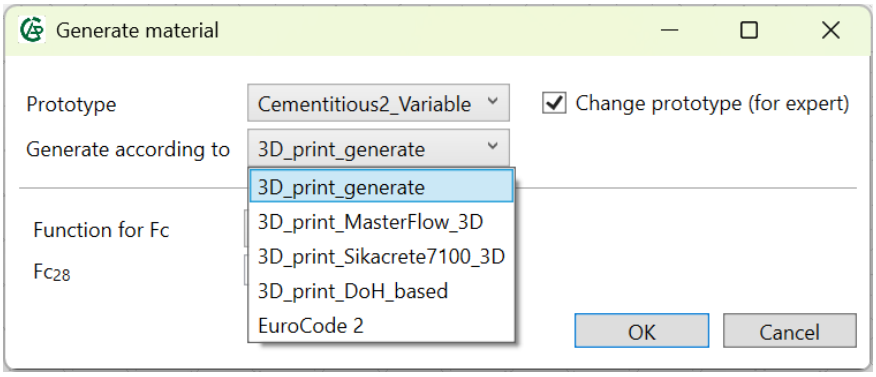

Figure 12: Generation of a new material model based on the Cementitios2_variable prototype that is suitable for 3D concrete printing.

Currently, there are three methods of generating the time-dependent parameters of the 3DCP material:

- Based on the development of compressive strength,
- Based on the development of the degree of hydration (DoH).
- Predefined materials Masterflow and Sikacrete.

The method for strength-based generation that relies on user input of the time-evolution of compressive strength given by a function $f_c(t)$. Based on this function, the time evolution of the remaining parameters of the fracture-plastic material model are deduced using relations summarised in Table 1.

Table 1: Relations for automatic generation of the time evolution of material properties for the fracture-plastic material model.

Parameter: symbol [unit]	Formula
Young's modulus: E [MPa]	$(6000 - 15.5f_{c,28})\sqrt{f_c}$
Tensile strength: f_t [MPa]	$3.5[f_c(t)/f_{c,28}]^{\frac{2}{3}}$
Specific fracture energy: G_f [N/m]	$73f_c(t)^{0.18}$
Critical compressive displacement: w_d [mm]	- 0.25
Onset of non-linearity in compression: f_{c0} [MPa]	$f_c(t)/3$
Plastic strain at compressive strength: ε_{cp} [-]	$f_c(t)/E_{28}$

Another option is to input the time evolution of the degree of hydration given by a function $\alpha(t)$. This is then translated to the evolution of the relative compressive strength through:

$$f_{c,rel}(t) = g(\alpha(t)) \ , \tag{1}$$

where the function $g(\alpha)$ is a mapping function converting the degree of hydration into the relative compressive strength. Function $g(\alpha)$ can be user-modified to reflect different mechanisms of strength increase in the early and mature state of the 3DCP material.

The relative compressive strength $f_{c,rel}(t)$ is scaled to compressive strength using a final, mature-state value. The other parameters for the material modelare again obtained using the relations in Table 1.

The main advantage of the DoH-based approach is that the hydration curve can be recalculated based on the material's temperature using the well-known Arrhenius law, scaling the hydration kinetics as follows:

$$\frac{\partial \alpha}{\partial t} = \left.\frac{\partial \alpha}{\partial t}\right|_{T=T_{ref}} exp\left[\frac{E_a}{R}\left(\frac{1}{T_{ref}} - \frac{1}{T}\right)\right] \quad , \tag{2}$$

where E_a is the activation energy, R is the universal gas constant, and T and T_{ref} are the actual and reference temperatures, respectively.

Once confirmed, the time-dependent functions for the parameters of the nonlinear material model are automatically generated. These parameters include the compressive and tensile strengths, Young's modulus, fracture energy, onset of crushing (i.e., nonlinear behaviour in compression), and plastic strain at compressive strength. An example is shown in Figure 13. The time-dependent functions for each parameter can be reviewed and adjusted to better fit the experimental data or expected material response. Finally, the material model is assigned to the bounding box solid.

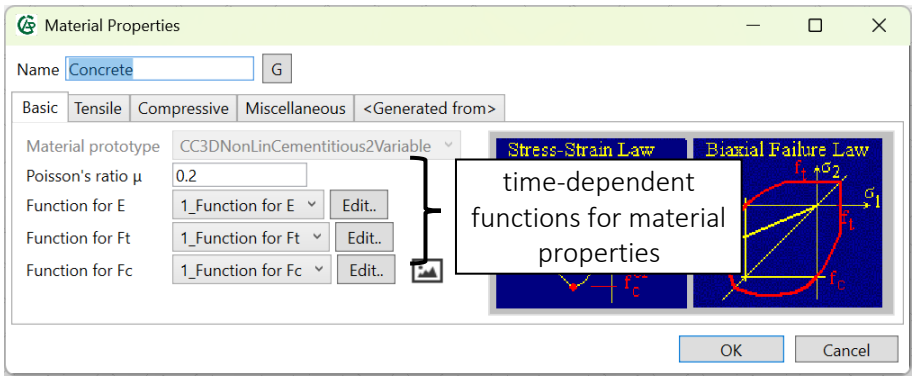

Figure 13: Definition of the time-dependent functions for material properties.

5.2.2 Interlayer interface model

Besides a concrete material model, an interface material can be assigned to the bounding box of the G-code FE model. If so, an interface connection is modelled between the adjacent concrete layers. If the interface model is not assigned to the bounding box solid, a fix connection through master-slave contacts is simulated between the layers.

To simulate a time-dependent evolution of the interface properties, there is a material model that allows variation of the material parameters during the analysis run. Similar to the concrete model described earlier, it updates the material properties of the interface based on the current step/time in the analysis. The definition includes the constant value of the parameter and a scaling function that modifies the constant value as a function of time. The input dialogue is shown in Figure 14.

It is recommended to scale the interface's normal and tangential stiffnesses proportionally to the evolution of the concrete's Young's modulus, while the cohesion and tensile strength should be scaled proportionally to the concrete's strength. The friction coefficient can be considered constant during the analysis run.

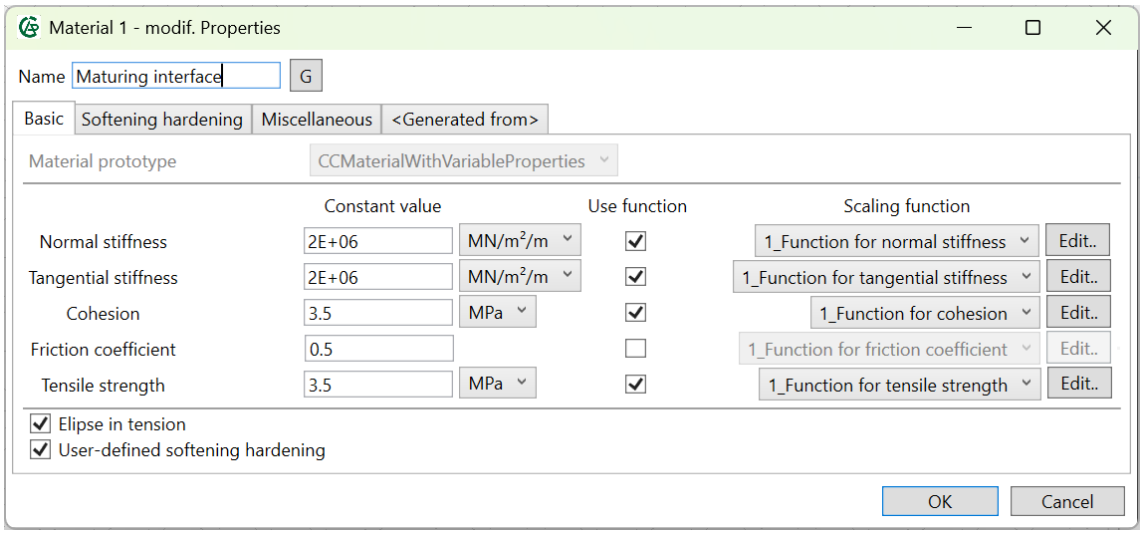

Figure 14: Definition of the time-dependent interface material.

5.3 Choosing fine element type

The FE mesh created from a G-code file utilises hexahedral elements. Other element shapes are not supported. The hexahedral elements can be used either with linear or quadratic shape functions. This setting is available in the building element window accessed under the **Building element types** option in the navigation tree.

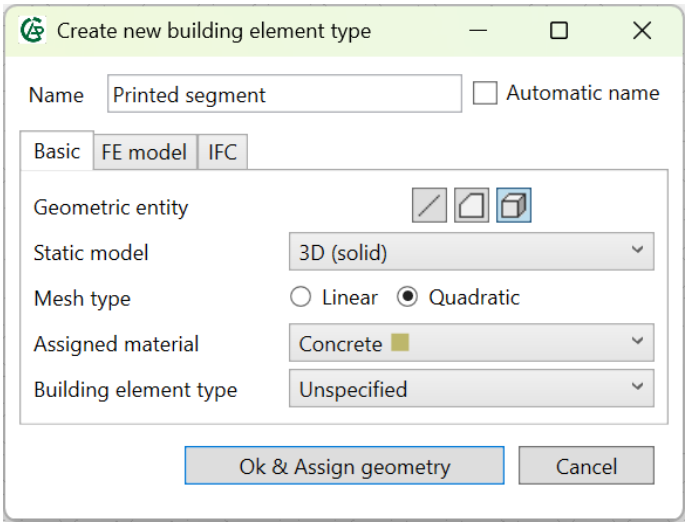

Figure 15: Input dialogue for element type settings.

For a more accurate stability analysis, the geometrical nonlinearity can be activated in the **FE model** tab. If the geometrical nonlinearity is not activated, the software still updates the nodal coordinates after each solution step, efficiently capturing the second-order effects. However, when the geometrical nonlinearity is activated, there is an additional inter-step update of the nodal coordinates even inside of a single solution step. Furthermore, the directions of the state variables are transformed according to the deformed shape when the geometrical nonlinearity is activated. For further information, please refer to the ATENA Theory manual [1], chapter 1.6 The Principle of Virtual Displacements.The assignment of the element type is not given to the FE model itself, but should be given to the bounding box solid.

5.4 Selections and boundary conditions

Similar to the assignment of the material model, the bounding box solid serves for prescribing the boundary conditions that should be applied to the surfaces or volume of the bounding box solid. In the case of 3DCP, these are mainly the supports, self-weight, and initial strain for the application of shrinkage strains. The boundary conditions are not applied directly on the bounding box solid but on selections that are created first through **Analysis: Selections** in the navigation tree window.

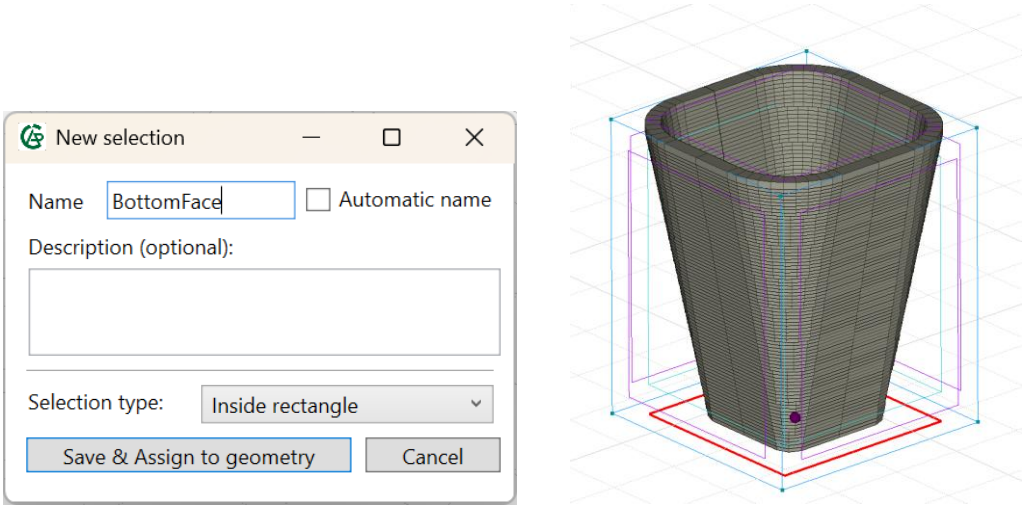

Figure 16: Creating a selection for nodes at the bottom face of the printed object for application of the support boundary condition.

The type of selection should correspond to the type of boundary condition that will be applied to this selection. For supports, typically applied on the bottom of the simulated elements, the selection should contain all nodes at the bottom face of the model. For this purpose, the **Selection type: Inside rectangle** should be used. It is prescribed to the bottom surface of the bounding box solid.

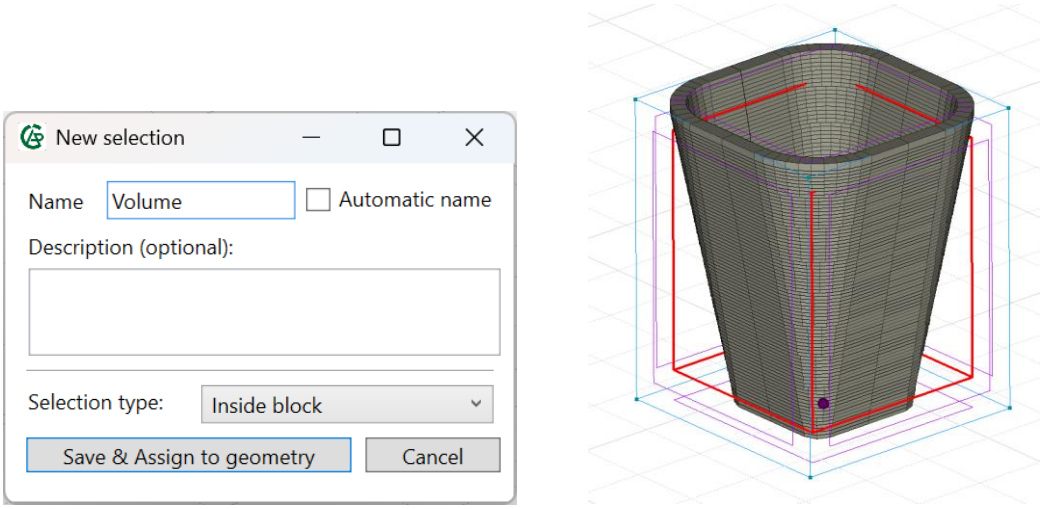

Figure 17: Creating a selection for all elements of the printed object for application of the self-weight.

The element self-weight and shrinkage loads are applied to the volumes, so the selection should include all elements of the FE model. These can be selected by **Selection type: Inside box**.

The boundary conditions are then created in a standard manner using the **Analysis: Boundary conditions** item in the navigation tree. For the supports, it is recommended to fix (i.e., constrain) all degrees of freedom on the bottom face of the model. It is important to note that the boundary conditions are assigned to the previously created selections and not directly on the volume or surfaces of the bounding box solid. This is done by activation of the **Use selection** option in the boundary condition window. The software then automatically ensures that the boundary condition is prescribed to the selection and that the type of the selection corresponds to the type of the boundary condition. An example of a dialogue for a support application is shown Figure 18 for supports and self-weight.

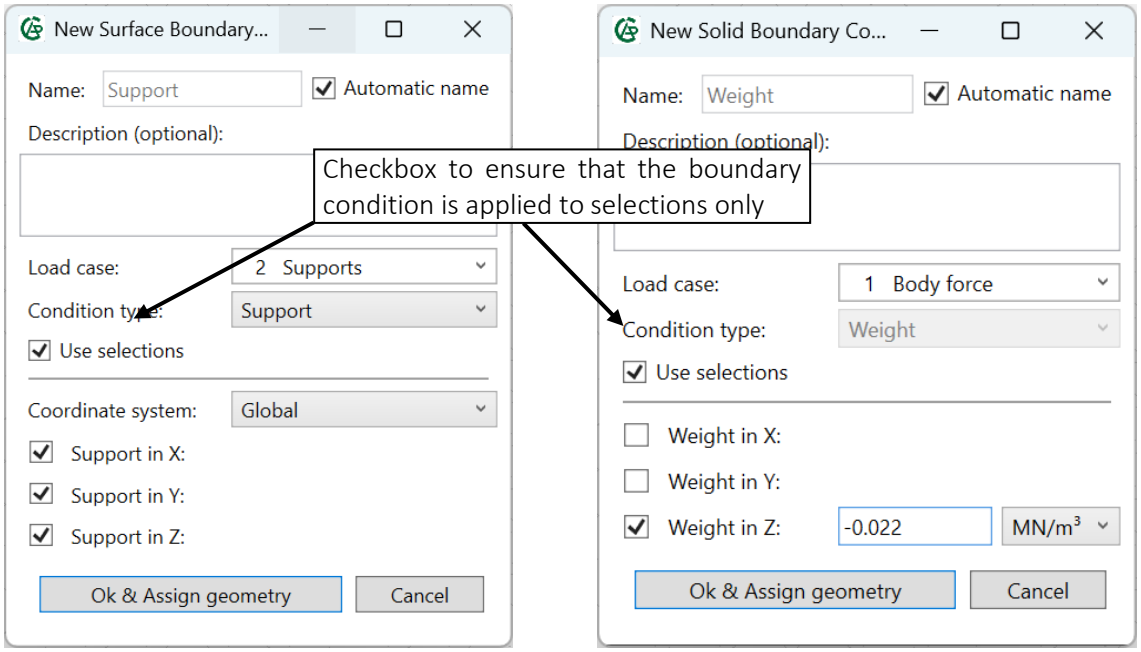

Figure 18: Definition of the support and self-weight boundary conditions applied to the previously defined selection.

5.5 Printing process definition

The 3D printing trajectory defines the spatial path of the print nozzle during material deposition and determines the geometry of the printed element. It represents a 1D curve in the 3D space derived from a digital. The associated printing velocity defines the speed of the printing nozzle, controlling the rate of material placement. In the 3DCP process, the trajectory and printing velocity play a key role in linking the digital design to the mechanical performance of the printed structure.

If the model is created through importing a G-code, the settings are mostly inherited from the **Create model from G-code** dialogue. These include the printing head trajectory or layer height and width. The settings can be reviewed in the **Trajectory properties** tab and even modified or overridden by a different G-code track.

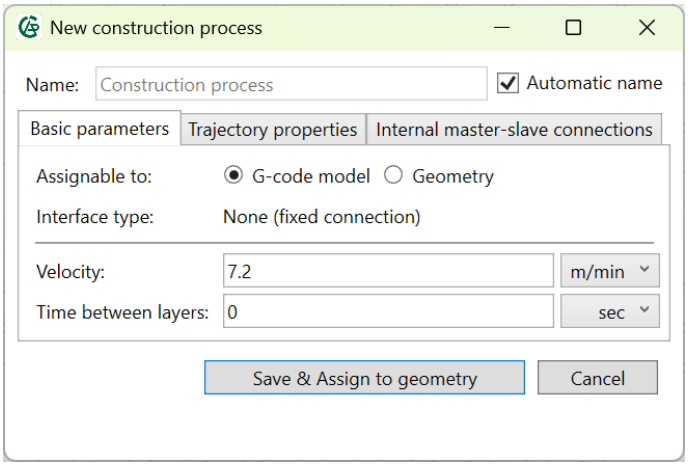

Figure 19: Creating a new construction process for 3D concrete printing.

5.6 Task settings

A 3DCP task is set similarly to the ordinary analysis. It includes the definition of the number of load steps and the selection of load cases. On top of that, a 3DCP task must include a relationship between the calculation step and the time. This is specified through activating the **Time definition** option in the interval settings and specifying the total duration of the interval. The time corresponding to each solution step is then used for updating the parameters of the material models and for activation of the finite elements along the printing path.

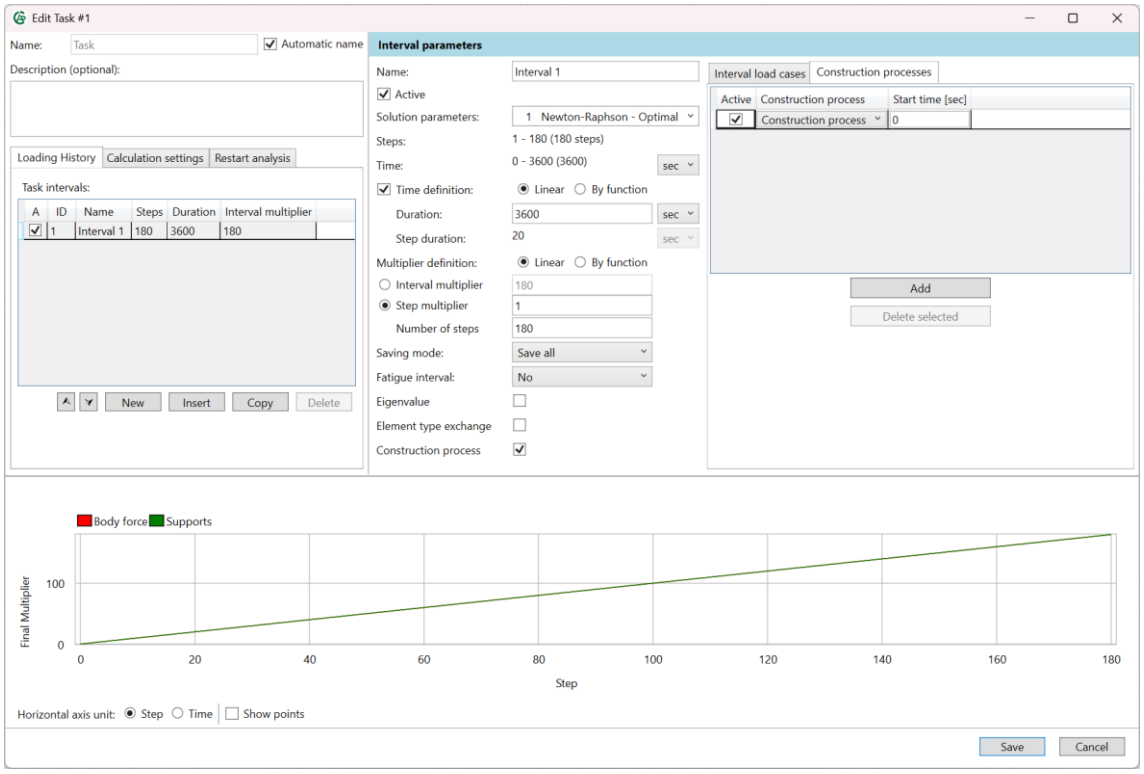

Figure 20: Task settings for a 3D printing simulation.

For the simulation of the 3DCP, the step multiplier should be activated and set to 1.0. This will ensure that the full value of the prescribed self-weight is applied to the elements

at the step when they are activated. When the self-weight boundary condition is applied to a solid with a construction process assigned, the load is applied only once at the moment of the element activation.

Before the first solution step, ATENA calculates the activation time of each finite element based on the printing trajectory and printing velocity. The elements are then gradually activated to simulate the printing as well as the parameters of the material model are updated.

The previously defined construction process needs to be added to the interval settings. To do so, the option **Construction process** is activated using a checkbox and the construction process with the printing settings is added to the table in the corresponding tab. An example of task settings is shown in Figure 20.

6 MODULE VALIDATION

6.1 Example 1: Buckling of a box element

6.1.1 Geometry

The validation of the presented module was conducted using experimental data obtained in the Klokner Institute, Prague. In the experiment, a box-shaped segment with a length of 2000 mm and a width of 200 mm was printed. No stiffening was used along the length of the segment since the goal of the experiment was to observe a buckling collapse during the printing process. Further experimental details are summarised in Table 2.

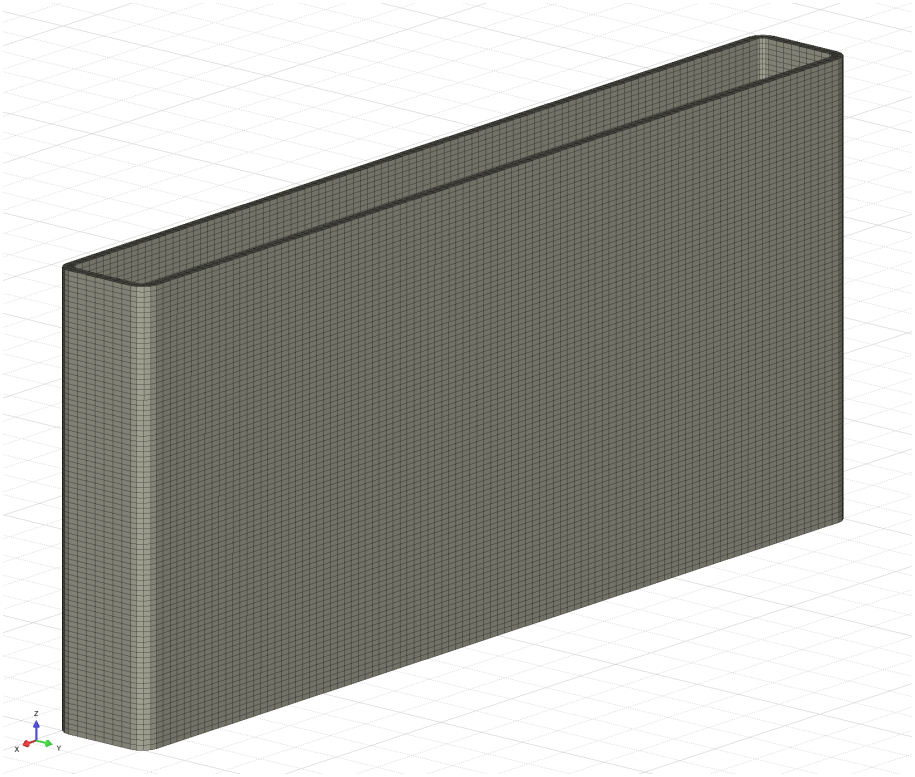

Figure 21: Overview of the finite element model of the box segment.

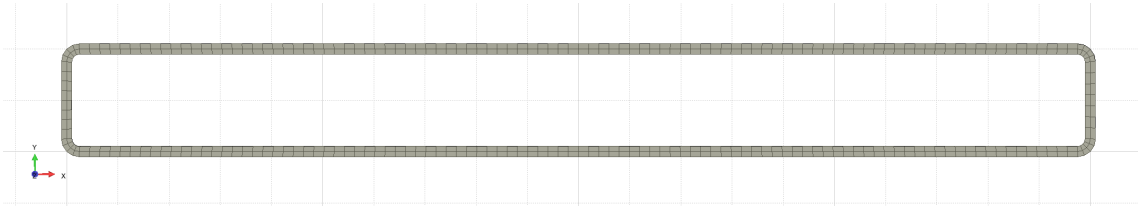

Figure 22: Top-view of the finite element model of the box segment.

The finite element model generated by the digiBeton module is shown in Figure 21 and Figure 22. The model is discretised using solid elements with quadratic approximation. The geometrical nonlinearity was activated for the elements, meaning the nodal coordinates are being updated during the iteration process within a single solution step and the state variables are transformed according to the elements' deformed shape.

The self-weight of the material was assumed 0.023 kN/m^3, which, as a body load, represents the loading in the simulation. The FE model was supported at the bottom face by fixing all degrees of freedom. The printing process was discretised into regular time steps, each having 20 s.

Table 2: Summary of experimental details.

Geometry	
total length	*2000 mm*
total width	*200 mm*
total height	*900 mm*
corner radius	*25 mm*
layer width	*20 mm*
layer height	*10 mm*
Printer settings	
printing velocity	*120 mm/s*

6.1.2 Material properties

The material properties were defined considering the experimental results measured on the paste with the same mixture proportion [5]. These include the time evolution of and heat of hydration, compressive strength, and Young's modulus and are plotted in Figure 23 and Figure 24.

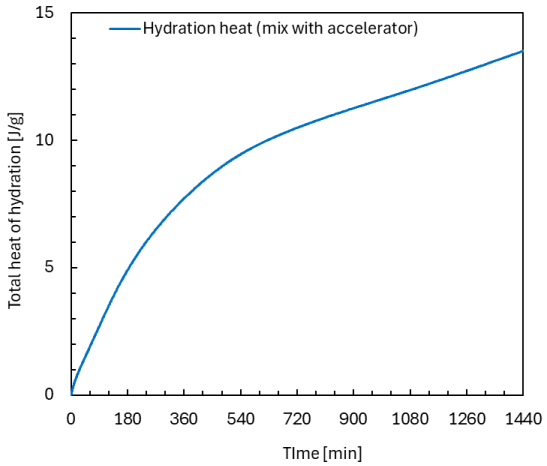

Figure 23: Heat of hydration for the used paste in the first 24 hours after mixing.

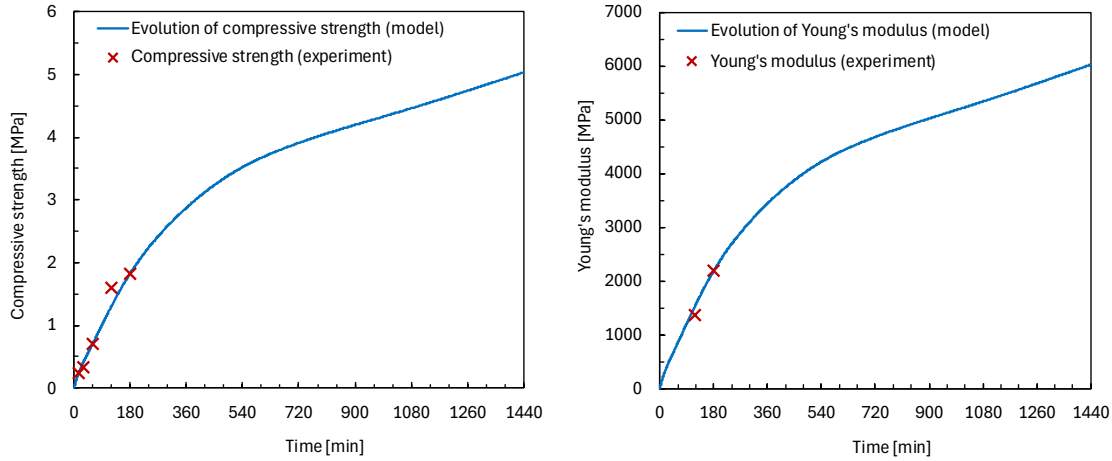

Figure 24: Evolution of compressive strength and Young's modulus in the first 24 hours after mixing.

The heat of hydration was measured continuously using isothermal calorimetry, while the material performance characteristics were obtained at several distinct ages of the material. For the purposes of the numerical analysis a continuous functions for the compressive strength and Young's modulus are needed; therefore, they were obtained using the heat of hydration curve as follows:

$$f_c(t) = \hat{Q}(t)\frac{\hat{f}_c(t_i)}{\hat{Q}(t_i)} \quad , \tag{3}$$

$$E(t) = \hat{Q}(t)\frac{\hat{E}(t_i)}{\hat{Q}(t_i)} \quad , \tag{4}$$

where $f_c(t)$ and $E(t)$ are the time-dependent compressive strength and Young's modulus functions, respectively, and $\hat{Q}, \hat{f}$, and $\hat{E}$, are the experimental values for the heat of hydration, compressive strength, and Young's modulus, respectively, measured at time t_i. For the remaining parameters that are needed for the material model, relations summarised in Table 3 were used.

Table 3: Relations for the time-dependent concrete material model.

Parameter: symbol [unit]	Formula
Tensile strength: f_t [MPa]	$3.5[f_c(t)/f_{c,28}]^{\frac{2}{3}}$
Specific fracture energy: G_f [N/m]	$73f_c(t)^{0.18}$
Critical compressive displacement: w_d [mm]	- 0.25
Onset of non-linearity in compression: f_{c0} [MPa]	$f_c(t)/3$
Plastic strain at compressive strength: ε_{cp} [-]	$f_c(t)/E_{28}$

The material parameters for the interface were estimated and are summarised in Table 4. These are estimates at the mature state and scaled using time-dependent functions either for stiffness or strength, based on the nature of the material property. The strength and

stiffness scaling functions are deduced from the evolution of the concrete compressive strength and Young's modulus using the following relations:

$$s_f(t) = \frac{f_c(t)}{f_{c,28}} \quad , \tag{5}$$

$$s_k(t) = \frac{E(t)}{E_{28}} \quad , \tag{6}$$

where $s_f(t)$ and $s_k(t)$ are the time-dependent strength and stiffness scaling functions, respectively, and $f_{c,28}$ and E_{28} are the concrete compressive strength and Young's modulus values at the matured state, respectively. The scaling function in Eqs. (5) and (6) are plotted in Figure 25.

Table 4: Parameters for the time-dependent interface material model.

Parameter: symbol [unit]	Value at 28-days	Scaling function
Cohesion: c [MPa]	3.5	strength evolution
Friction coefficient: μ [-]	0.5	constant
Tensile strength: $f_{t,i}$ [MPa]	3.5	strength evolution
Normal stiffness: k_{nn} [MPa/m]	3.67×10^6	stiffness evolution
Tangential stiffness: k_{tt} [MPa/m]	3.67×10^6	stiffness evolution

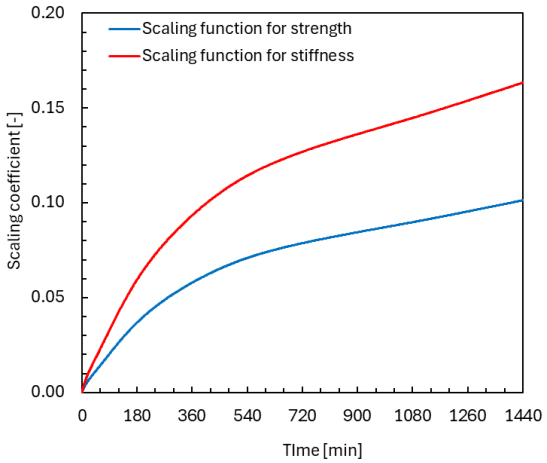

Figure 25: Scaling functions used for the interface material.

6.1.3 Results and discussion

The results of the initial simulation are shown in Figure 26 plotting displacement in the lateral direction. The model did not collapse during this simulation, revealing only negligible deflection over the length of the wall.

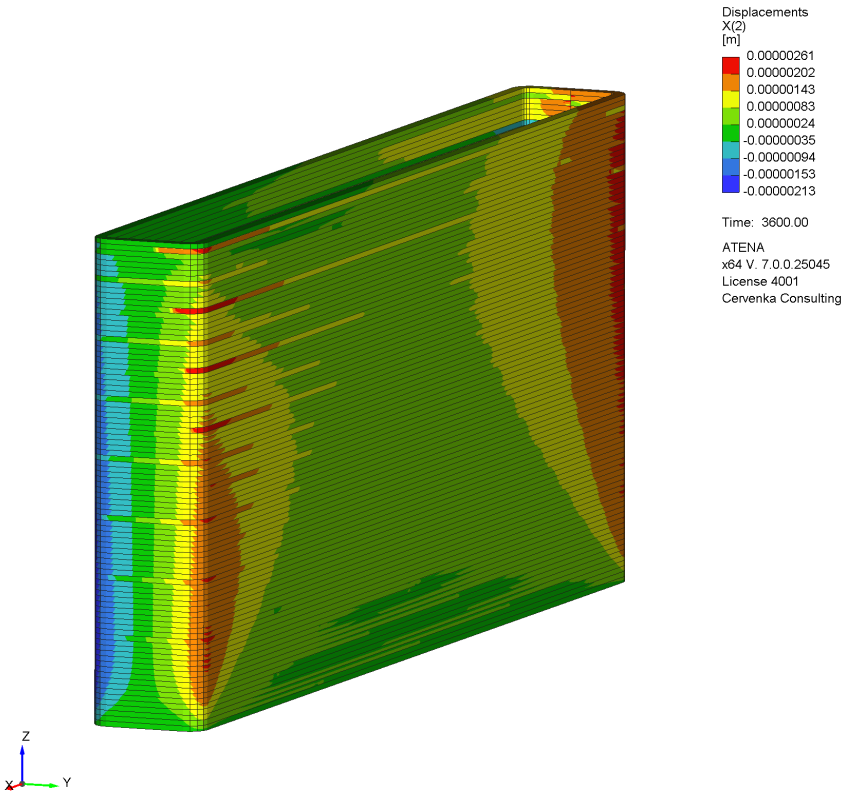

Figure 26: Results of the simulation of the 3D concrete printing process of the box element with initial material properties.

Based on the initial results, a parametric study was conducted to fit the numerical results to the behaviour observed in the experiment. As the fitting parameter, the time evolution of the Young's modulus was chosen as it directly affects the stiffness of the element under printing and thus the buckling resistance.

In Figure 27, the results with an initial value of Young's modulus scaled by 1 % are shown. It shows buckling of the wall segment at a height of 380 mm. The buckling develops gradually and is accelerated by the deposition of subsequent layers. A comparison with the behaviour observed in the experiment is shown in Figure 28.

The discrepancy in the Young's modulus value in the model and measured in the experiment can be interpreted as the experimental value representing an upper-bound performance, while the actual material performance when printed is altered by environmental and printing factors.

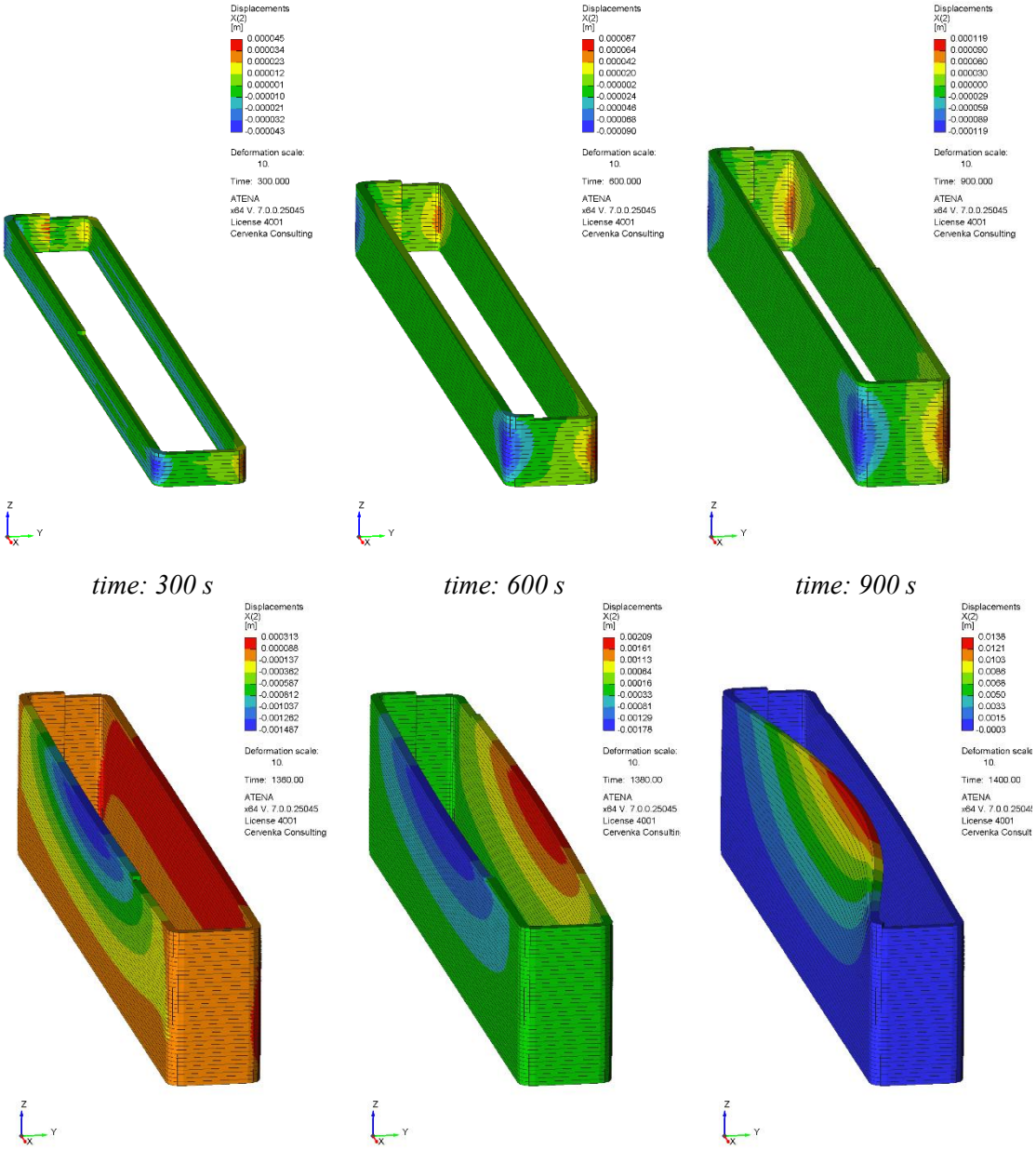

time: 300 s *time: 600 s* *time: 900 s*

time: 1360 s *time: 1380 s* *time: 1400 s*

Figure 27: Box segment with a reduced Young's modulus at different stages of printing. The deflection in the straight segment gradually develops, leading to buckling collapse.

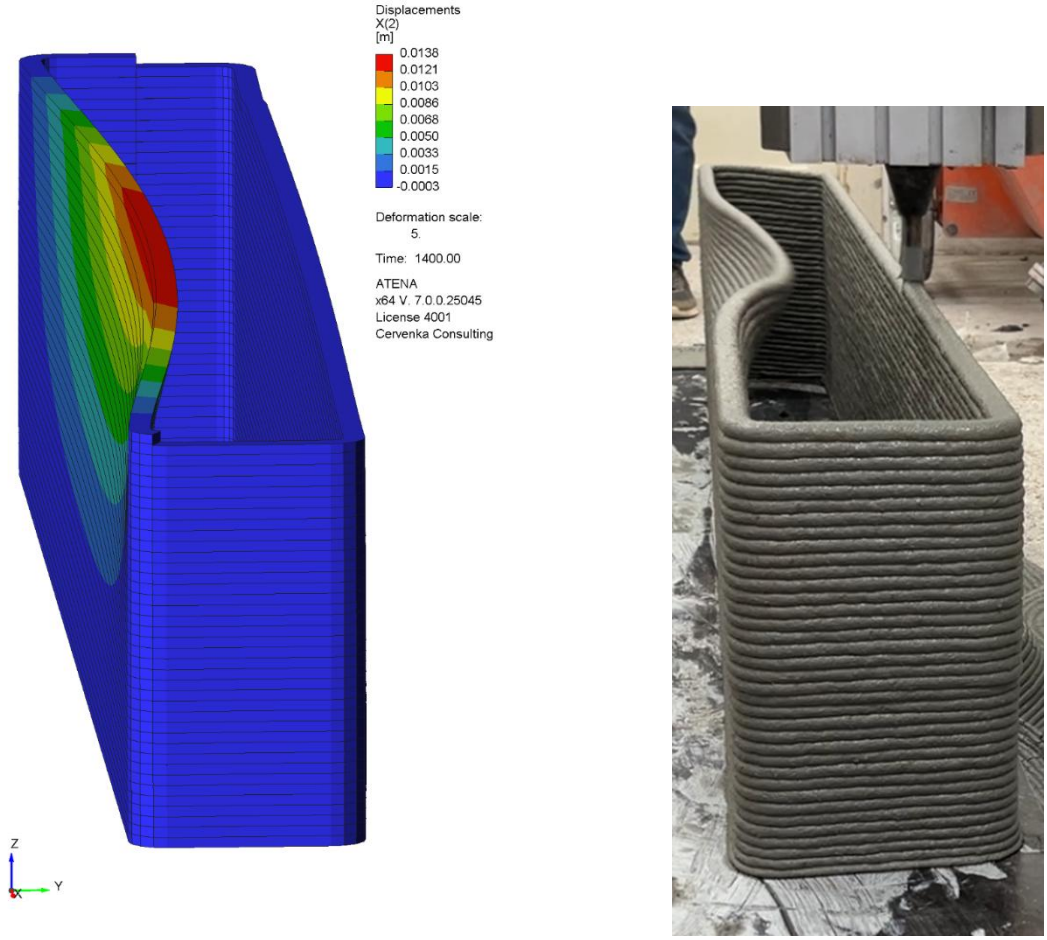

Figure 28: Comparison of the results from the numerical simulation with reduced Young's modulus (left) with the experiment (right).

6.2 Example 2: Prvok House

6.2.1 Introduction

The simulation framework of the digiBeton module was further adopted in the simulation of the printing process of the Prvok House, built in Prague, Czech Republic. The name "Prvok," translating to "Protozoan" in English, holds a dual meaning. It signifies the first large-scale application of 3DCP in the Czech Republic, while also referencing the house's design, which evokes the shape of these early single-celled organisms.

The Prvok House features a sandwich wall structure consisting of an outer and inner surface connected by stirrup reinforcement. Each printed layer is 45 mm thick and 12 mm high. The outer wall's distinctive wavy geometry not only provides an interesting architectural aesthetic but also enhances its out-of-plane stability. In contrast, the inner wall lacks the wavy design; however, its stability is provided by sigma-shaped columns spaced approximately every half meter. A photo of the Prvok House after construction is shown in Figure 29.

Figure 29: The Prvok House after printing in the city center of Prague, Czech Republic (courtesy of Scoolpt s.r.o.).

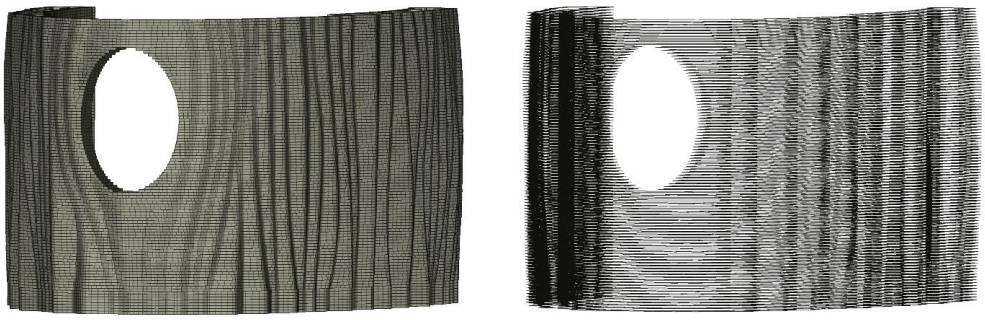

Figure 30: Finite element model of the Prvok House: (left) Solid elements for concrete and (right) Interface elements printed between layers.

6.2.2 Numerical model

The finite element model represents one-half of the whole structure, including the elliptical window in the front. The model is shown Figure 30.

The simulation of the 3DCP process considers the actual building sequence as follows: First, the entire length of the wall base was printed until the height of the front window. Second, the wall section on the left side of the window was constructed up to the top of the window opening, followed by the corresponding section on the right. Lastly, the entire section of the sandwich wall above the window was printed. The analysis assumed a total construction time of approximately 90 hours. The model employs interfaces automatically generated between the printed layers, which typically represent a weak spot in structures constructed by 3DCP.

6.2.3 Analysis results

The analysis results showing the principal compressive strain at various stages of the printing are given in Figure 31. It can be seen that a larger compressive strain is predicted on both sides of the window opening compared to the wall below and above the opening. This originates from the construction method when the segments on the left and right sides of the wall were printed as two individual segments, while the wall below the opening was printed in one piece. Therefore, the construction speed for printing the lower segment was approximately half that of the rest of the structure. Due to higher construction speed, the material there is younger, thus having lower mechanical performance characteristics when the subsequent concrete layers are deposited. This results in higher deformation and higher strain.

For the construction, a commercially available, ready-to-use fiber-reinforced concrete mix specifically formulated for 3DCP was used. The technical specifications provided by the manufacturer were used to estimate the parameters for the kinetic material model used in the simulation.

Furthermore, as no additional support was modelled at the front opening, cracks with a maximum width of 0.6 mm are predicted in this region as illustrated in Figure 32. It should be noted that these cracks originate only from the mechanical loading, as all shrinkage was neglected in this analysis.

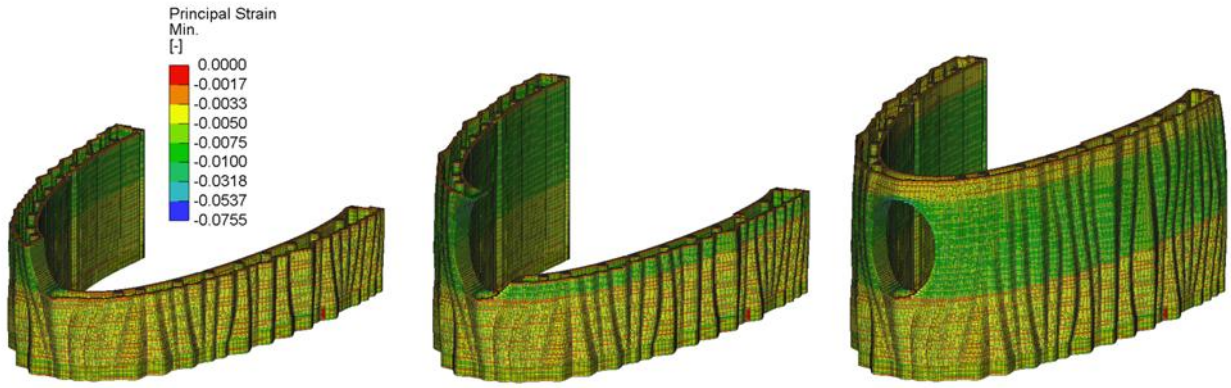

Figure 31: Principal compressive strain at various stages of the printing of the Prvok House.

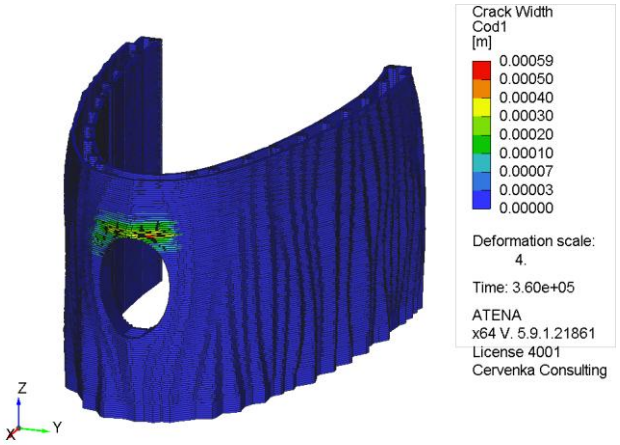

Figure 32: Crack pattern and crack width above the opening.

6.3 Example 3: Wall segment

6.3.1 Experimental and Numerical Methods

As part of the experimental program, a 3DCP wall segment with base dimensions of 300 × 970 mm and a height of 800 mm was prepared at the Klokner Institute, Prague, Czech Republic. The width of the printed layer was 20 mm and height 10 mm. The printing speed in the analysis was assumed to be 120 mm/s.

Along the longer edge, the wall segment was stiffened by inner stiffeners for better overall mechanical performance. The compressive strength of the material used for printing is 50 MPa at 28 days. A photo of the element after the printing is shown in Figure 33. After maturing, the wall segment was subjected to compressive strength to determine its load-bearing capacity.

Figure 33: Photo of the 3D-printed wall segment.

A finite element model was developed to reproduce the results of the experimental program. The model of the wall segment consisted of 27 680 elements with quadratic approximation, each having 3 degrees of freedom. The mesh of the wall segment is shown in Figure 34 (left). To capture the anisotropy in the structure due to 3DCP, horizontal interface elements were modelled between every layer. Furthermore, a vertical interface was modelled inside the two inner stiffeners. The geometry of the interfaces is shown in Figure 34 (right) together with the loading plate modelled for the application of the vertical displacement during the load test simulation.

The development of the compressive strength was based on the experimental data, which were available from the material age of 15 minutes. The values of time development of the Young's modulus, which are important for the deformation during printing, were not available for the young material; therefore, they were assumed to develop exponentially between age 0 min and the measured values at the ages of 2 and 3 hours. The initial value of Young's modulus at time 0 min was taken as 0.153 MPa same as for the material presented in the study of Esposito et al. [6]. The assumed evolution of the compressive strength, Young's modulus, and tensile strength over time are plotted in Figure 35. The interfaces properties are summarised in Table 5.

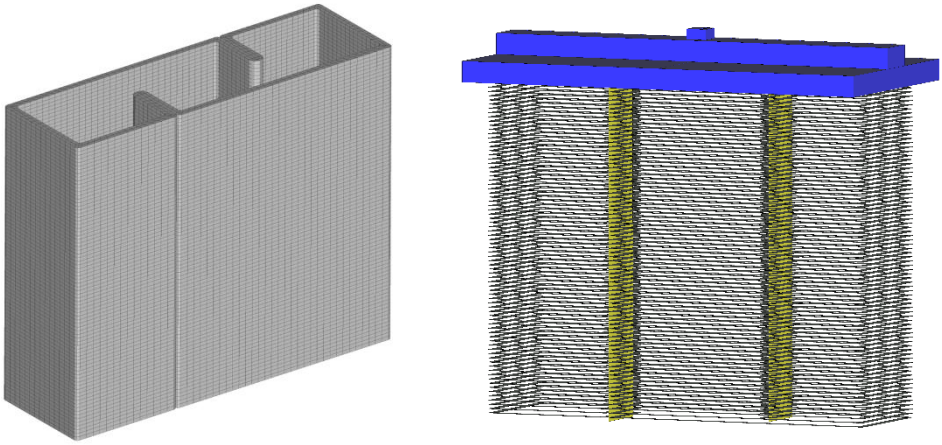

Figure 34: Numerical model of the wall segment: Finite element mesh of the concrete elements (left) and Geometry of the horizontal (i.e., interlayer) and vertical interfaces together with the geometry of the loading plate (right).

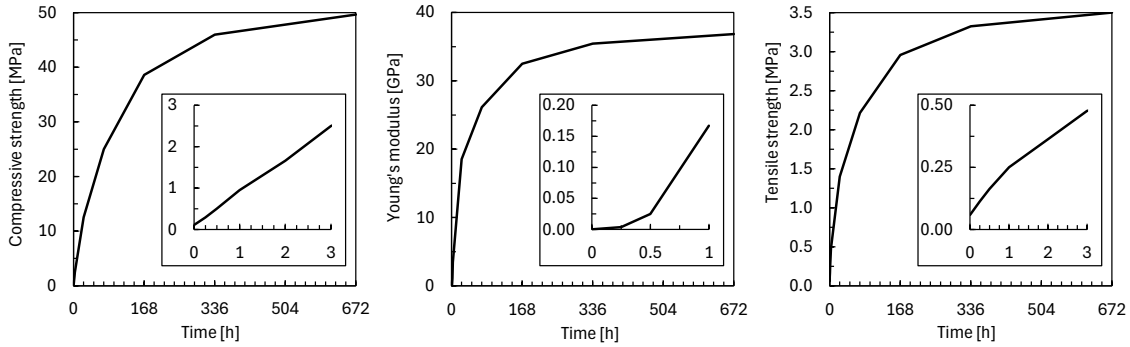

Figure 35: Development of the mechanical properties of the fresh concrete material: (a) Compressive strength (left), Young's modulus (center), and Tensile strength (right). The details show the development at an early age.

Table 5: Material parameters of the interfaces used in the numerical model.

Parameter: symbol [unit]	Horizontal interface (interlayer)	Vertical interface (in the inner stiffener)
Tensile strength: $f_{t,int}$ [MPa]	0.50	0.25
Cohesion: c [MPa]	0.50	0.25
Friction coefficient: μ [-]	0.5	0.5

6.3.2 Results and Discussion

The displacement showing a gradual buckling of the printed element is shown in Figure 36 for 15, 25, and 30 minutes of the printing process. From the numerical results, the maximum out-of-plane deformation at the end of the printing process reached 5.5 mm in the longer portion of the longitudinal wall. This deformation enters the simulation of the compression test as an initial imperfection.

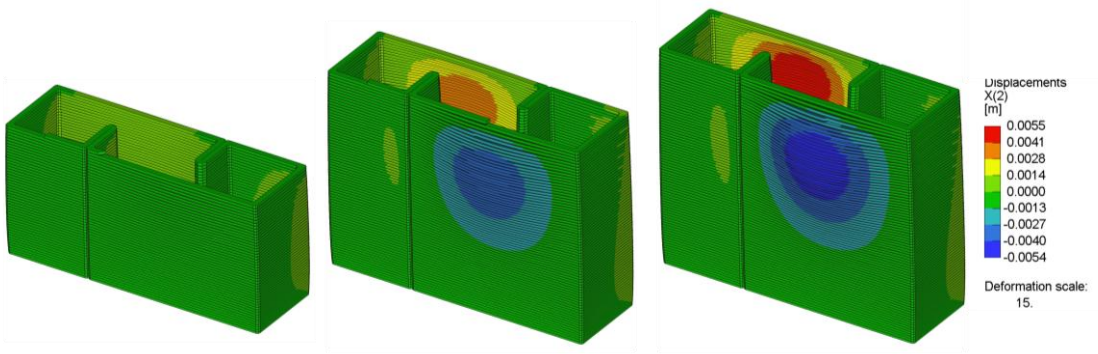

Figure 36: Out-of-plane displacement perpendicular to the longitudinal dimension of the wall showing gradual buckling at 15 minutes (left), 25 minutes (center), and (right) at the end of printing at 30 minutes (deformation scale ×15).

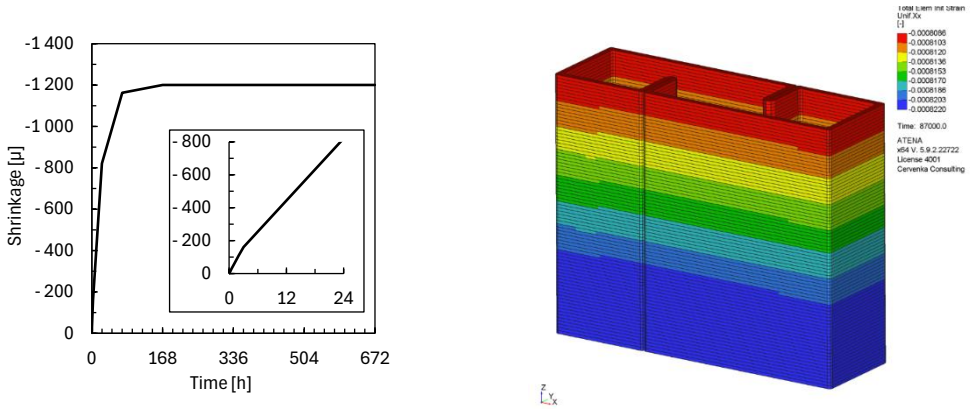

Figure 37: Shrinkage load applied on the model: Shrinkage evolution in time (left) and Differential shrinkage strain on the model at the time of 1 day (right).

In the simulation, the shrinkage strain of -1200 μ was applied to the model in the form of initial strain. The evolution of the shrinkage used in the analysis is plotted in Figure 37 (left) and the distribution of the initial strain in the model is shown in Figure 37 (right) at the time of 1 day. The shrinkage load did not result in any crack formation in the simulation.

A loading test was simulated at the age of 28 days. Figure 38 shows a comparison between the load-displacement diagram measured in the experiment and the analysis results. It shows a good agreement both in the peak load and stiffness. The maximum load measured in the experiment was 818 kN, while the model predicted failure at 764 kN. For comparison, another analysis that neglected the interlayer and vertical interfaces as well as the construction processes, was conducted. This analysis gave the maximum loading capacity of 2044 kN. Therefore, neglecting the weaker interlayer bond and imperfection from the printing process resulted in an overestimation of the actual load-bearing capacity by 168 %.

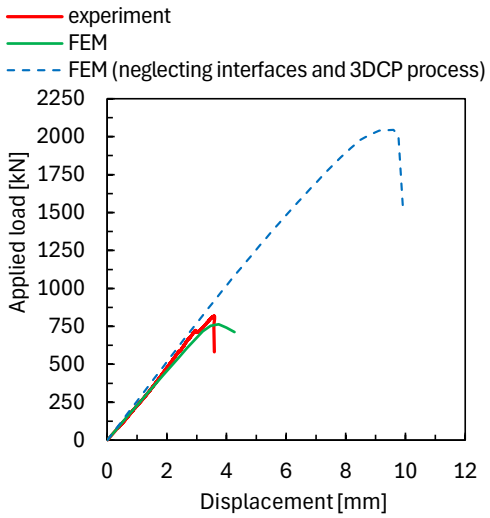

Figure 38: Comparison of the load-displacement diagram from the experiment and analyses. The blue dashed curve shows analysis results neglecting interfaces and the simulation of the printing process, thus having no initial imperfection.

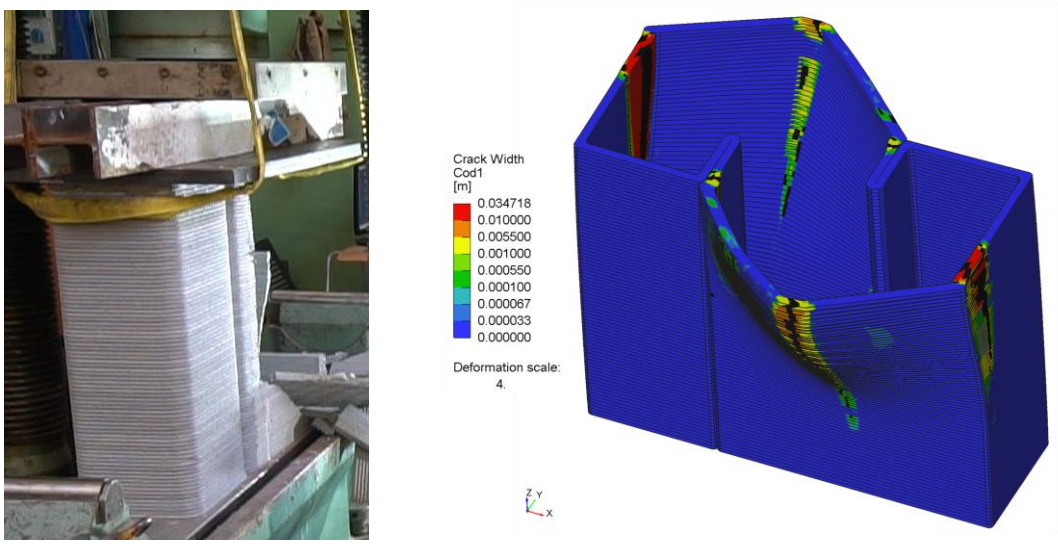

Figure 39: Post-peak failure mode: Experimental results (left) and Crack width in the numerical results (deformation scale ×4, only cracks larger than 0.1 mm are emphasised) (right).

The simulation results showed a similar failure mechanism to that in the experiment. As the load increases, the horizontal deformation in the longer portion of the longitudinal wall increases. This is associated with crack formation at both ends of this wall portion and at its center. Finally, at the peak load, this part of the element undergoes out-of-plane brittle collapse. The failure modes observed in the experiment and in the numerical analysis are shown in Figure 39. For comparison, the failure model observed in the analysis neglecting the interfaces and the simulation of the 3DCP process is plotted in Figure 40.

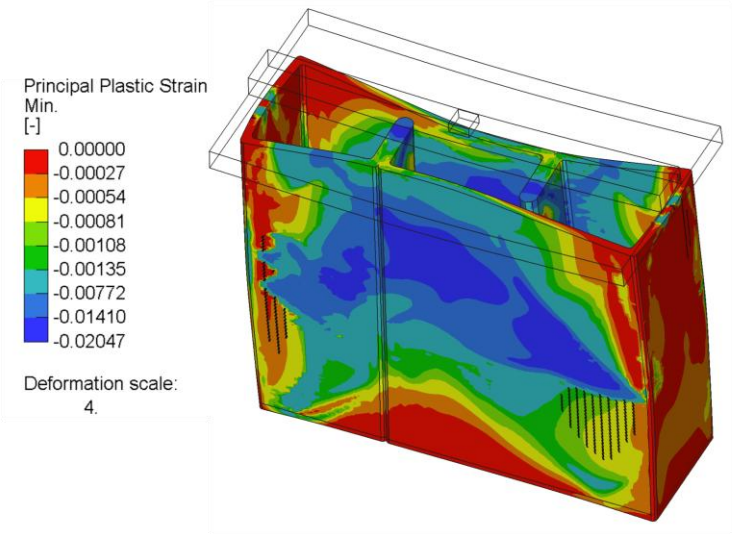

Figure 40: Post-peak failure mode in the model neglecting interfaces and the simulation of the 3DCP process (deformation scale ×4, only cracks larger than 0.1 mm are emphasised).

6.3.3 Conclusions

This example presents a complex non-linear FEM analysis assessing the structural behaviour of a 3DCP element, both at the early and mature ages. The analysis relies on a time-dependent material model allowing for simulating the change in the nature of the material from the fresh paste to the hardened concrete. First, the concrete printing process was simulated through the gradual activation of the finite elements along the printing trajectory. This allowed assessment of the stability during construction. Weaker interlayer bonds between the printed layers were captured through interface elements within the model. The calculated deformation in the early age was kept in the model and influenced the structural performance during the load test simulation in the mature age. By comparing the load-displacement curves and failure modes obtained from the analysis and experiment, the ability of the FEM model to reproduce actual mechanical behaviour was validated.

The numerical model was further used to calculate the idealised maximum load-bearing capacity of the element when assuming a perfect interlayer bond and no initial imperfection. The analysis suggested that, in the particular case of this element, neglecting these important aspects of the 3DCP structure may lead to an overestimation of the actual load-bearing capacity by 168 %.

These findings highlight the critical importance of considering the unique characteristics of additively manufactured elements for accurate load-bearing capacity assessments. Furthermore, the potential of non-linear FEM for comprehensive evaluations of the structural integrity of 3DDCP elements from the early to mature age.

REFERENCES

[1] Červenka, V., Jendele, L, Červenka, J., (2025), *ATENA Program Documentation, Part 1, Theory*. Červenka Consulting.

[2] Červenka, J., Červenka, V., Eligehausen, R., (1998), *Fracture-plastic material model for concrete, application to analysis of powder actuated anchors*. in: Proc. Fram., pp. 1107–1116.

[3] Červenka, J., Papanikolaou, V.K., (2008) *Three dimensional combined fracture–plastic material model for concrete*. Int. J. Plast. 24 2192–2220. https://doi.org/10.1016/J.IJPLAS.2008.01.004.

[4] Menetrey, P., Willam, K. J., (1995). *Triaxial failure criterion for concrete and its generalization*. Structural Journal, 92(3), 311-318.

[5] Červenka, J. et al., (2024), *Odborná zpráva o řešení projektu FW06010422 Simulace a navrhování konstrukcí z digitálního betonu 2024.,*

[6] Esposito, L., Casagrande, L., Menna, C., Asprone, D., & Auricchio, F. (2021). *Early-age creep behaviour of 3D printable mortars: experimental characterisation and analytical modelling*. Materials and Structures, *54*(6), 207.